Environ Geochem Health (2016) 38:511–521
DOI 10.1007/s10653-015-9736-6

ORIGINAL PAPER

Chemically modified biochar produced from conocarpus waste increases NO_3 removal from aqueous solutions

Adel R. A. Usman · Mahtab Ahmad · Mohamed El-Mahrouky · Abdulrasoul Al-Omran · Yong Sik Ok · Abdelazeem Sh. Sallam · Ahmed H. El-Naggar · Mohammad I. Al-Wabel

Received: 26 February 2015 / Accepted: 16 June 2015 / Published online: 23 June 2015

Abstract Biochar has emerged as a universal sorbent for the removal of contaminants from water and soil. However, its efficiency is lower than that of commercially available sorbents. Engineering biochar by chemical modification may improve its sorption efficiency. In this study, conocarpus green waste was chemically modified with magnesium and iron oxides and then subjected to thermal pyrolysis to produce biochar. These chemically modified biochars were tested for NO_3 removal efficiency from aqueous solutions in batch sorption isothermal and kinetic experiments. The results revealed that MgO-biochar outperformed other biochars with a maximum NO_3 sorption capacity of 45.36 mmol kg^{-1} predicted by the Langmuir sorption model. The kinetics data were well described by the Type 1 pseudo-second-order model, indicating chemisorption as the dominating mechanism of NO_3 sorption onto biochars. Greater efficiency of MgO-biochar was related to its high specific surface area (391.8 m^2 g^{-1}) and formation of strong ionic complexes with NO_3. At an initial pH of 2, more than 89 % NO_3 removal efficiency was observed for all of the biochars. We conclude that chemical modification can alter the surface chemistry of biochar, thereby leading to enhanced sorption capacity compared with simple biochar.

Keywords Engineered biochar · Kinetics · Sorption capacity · Green waste · Chemical modification

A. R. A. Usman · M. Ahmad · M. El-Mahrouky · A. Al-Omran · A. Sh. Sallam · A. H. El-Naggar · M. I. Al-Wabel (✉)
Soil Sciences Department, College of Food and Agriculture Sciences, King Saud University, P.O. Box 2460, Riyadh 11451, Saudi Arabia
e-mail: malwabel@ksu.edu.sa

A. R. A. Usman
Department of Soils and Water, Faculty of Agriculture, Assiut University, Assiut 71526, Egypt

Y. S. Ok
Korea Biochar Research Center, Kangwon National University, Chuncheon 200-701, Korea

A. H. El-Naggar
Department of Soil Science, Faculty of Agriculture, Ain Shams University, 68 Hadayek Shobra, P.O. Box 11241, Cairo, Egypt

Introduction

Biochar is a carbon-rich product obtained by heating biomass such as wood, manure or leaves in a closed system with little or no air (Lehmann and Joseph 2009). Multidisciplinary actions of biochar have attracted researchers to work in a new era of science and engineering. Potential applications of biochar include soil fertility improvement, carbon sequestration, pollution remediation and waste recycling (Al-Wabel et al. 2013; Ahmad et al. 2014a). Sustainable production of biochar may limit its resources.

Therefore, biomass for biochar production should be devoid of other values such as food security, soil fertility and forest safety. Shackley et al. (2011) classified biomass into virgin and non-virgin. Virgin biomass is derived from plants and trees or their by-products that has not been subjected to any chemical or biological transformation or treatment, and any other biomass not falling under the definition of virgin biomass is non-virgin biomass (Shackley et al. 2011). Due to the associated contamination and potential pollution effects, non-virgin resources (sewage waste, poultry litter, food waste, etc.) are generally avoided for biochar production. The use of waste biomass (as a virgin biomass resource) has proven to be a cost-effective method of biochar production. Particularly, green waste comprising leaves, tree branches, logs and brush can effectively be converted to biochar. *Conocarpus erectus* L. (button wood), a widespread tree planted in Saudi Arabia, has been declared as problematic by the Municipal Council of the city of Riyadh because of its huge aboveground biomass (Al-Wabel et al. 2013). Thus, conocarpus waste was selected as a useful precursor for biochar production to eliminate recycling and management issues.

Recently, biochar has been successfully used as universal sorbent for the treatment of organically and inorganically contaminated water (Ahmad et al. 2012; Ahmad et al. 2013a, b; Usman et al. 2013; Rajapaksha et al. 2014; Mohan et al. 2014). However, it is less efficient compared with commercially available adsorbents such as activated carbon (Ahmad et al. 2012). Therefore, biochar needs to be engineered or modified to enhance its sorption efficiency. Generally, engineered biochar can be achieved by controlling the pyrolytic process and/or physicochemical modification (Vithanage et al. 2014; Mayer et al. 2014). Specifically, the chemistry of biochar can be modified by either treating the feedstock prior to biochar conversion or after the production of biochar. Various chemicals such as sulfuric acid and oxalic acid (Vithanage et al. 2014), magnesium hydroxide (Usman et al. 2013), polyethylene amine (Ma et al. 2014) and methanol (Jing et al. 2014) have been tested for biochar modification. These chemicals either increase the surface area or form surface functional groups that chemically bond with the contaminant. Ion exchange is another mechanism by which biochar surface can be modified with a cation or anion depending on the prevailing species of the contaminant. For instance, cation-modified biochar could be effective in removing phosphate (PO_4^{3-}) and nitrate (NO_3^-) from water. In general, cations such as magnesium (Mg^{2+}) and iron (Fe^{2+} or Fe^{3+}) can easily be attached electrostatically to the negatively charged biochar surface, which then facilitates complexation with negatively charged contaminants.

Nitrate pollution of water is a worldwide problem associated with the extensive use of nitrogen fertilizers and manure in agricultural fields (Liu et al. 2011; Ahmad et al. 2014b). Elevated NO_3 levels in drinking water are toxic to humans, causing methemoglobinemia in infants and cancer of the digestive tract (Keshavarzi et al. 2012; Camargo et al. 2005). Thus, a safe limit of 50 mg L^{-1} NO_3 in drinking water has been established by the World Health Organization (WHO 2011). Typically, in arid countries such as Saudi Arabia, where there are limited water resources, high concentrations of NO_3 (>180 mg L^{-1}) emanating from nitrogen fertilizers and sewage seepage have restricted groundwater use for drinking purposes (Loni et al. 2014; Metwaly et al. 2014). Furthermore, high NO_3 content (>200 mg L^{-1}) in industrial wastewater (Aly et al. 2014) poses a treatment challenge. It is therefore imperative to protect water resources by applying a suitable treatment technology for NO_3 removal. Various treatment technologies including biological denitrification, reverse osmosis, electrocatalysis and reduction processes have been employed (Wang et al. 2014). However, there are certain limitations of using these techniques. For example, biological methods are relatively slow and inefficient, and they generate excessive biomass (Kassaee et al. 2011); reverse osmosis and electrocatalysis need costly installations and maintenance (Rodríguez-Marotoet et al. 2009). Compared with these techniques, adsorption is reported to be one of the simplest and most efficient and economical techniques for removing NO_3 from water (Sowmya and Meenakshi 2014). Materials such as organo-clay, red mud, nanoalumina, ferric hydroxide and activated carbon have been widely examined as sorbents for NO_3 removal from aqueous media (Bagherifam et al. 2014).

Here, we proposed chemically modified biochar derived from conocarpus waste as a novel material for the remediation of NO_3-contaminated water. We hypothesized that the negatively charged surface of biochar can be modified by cations such as Mg^{2+} and

Fe^{2+} that will enhance the NO_3 removal efficiency of biochar, most likely as a result of chemisorption. To our knowledge, this is the first time that we report the sorption efficiency of chemically modified conocarpus biochar for the removal of NO_3 from water. No data are available on the kinetics and sorption isotherms of NO_3 on chemically modified biochar. The specific objectives of the study are: (1) the chemical modification of biochar derived from conocarpus waste with magnesium and iron oxides, (2) the application and comparison of un-modified and chemically modified biochars for the removal of NO_3 from water and (3) the determination of the interaction between NO_3 and biochar using various isotherm and kinetic models.

Materials and methods

Preparation, chemical modification and characterization of biochar

Conocarpus green waste collected from the King Saud University campus was dried under sunlight and then ground to a particle size of 7–10 cm. Proportions of the feedstock were subjected to chemical modification with either Mg or Fe salts by a method of chemical co-precipitation (Chen et al. 2011; Usman et al. 2013; Zhang et al. 2012). Specifically, the feedstock was saturated in 1 M $MgCl_2$ or 1 M $FeCl_2$/$FeCl_3$ solution for 2 h. Subsequently, the pH of the $FeCl_2$/$FeCl_3$ suspension was raised to 10 by slowly adding NaOH solution. The deposits were then separated, washed several times with deionized water and dried in an oven at 80 °C. Finally, un-modified conocarpus waste and Mg- and Fe-modified conocarpus wastes were pyrolyzed in a closed system in an outdoor cylindrical pyrolysis reactor (made of stainless steel) at 600 °C for 4 h. The resulting biochars were cooled inside the reactor chamber and then ground to <0.5 mm particle size. The biochar samples were rinsed several times with deionized water, dried at 80 °C overnight in an oven and transferred to air- and moisture-free closed vessels. The chemically modified biochars were hereafter named as MgO-biochar and FeO-biochar.

The surface structural characteristics such as surface area, pore volume, pore size and average particle size of un-modified and chemically modified biochars were measured by the Gemini VII 2390 series surface area analyzer (Micromeritics, USA). The samples were degassed for 1 h at 300 °C prior to analysis. The Brunauer–Emmett–Teller (BET) and the Barret–Joyner–Halender (BJH) equations were used to calculate the specific surface area, pore volume and pore size (Ahmad et al. 2012). A scanning electron microscope (SEM) (EFI, S50, Inspect, Netherlands) was employed to examine the surface morphology of the biochars. Additionally, X-ray diffraction (XRD) analysis (XRD-7000, Shimadzu Japan) was also carried out to identify mineral phase changes in the biochars. The spectral properties of the synthesized biochars were determined by the Fourier transform infrared (FTIR) spectrometer (Nicolet 6700, USA) using a wavelength range of 400–4000 cm^{-1}.

Kinetics study

To test the biochars for NO_3 removal from aqueous solution, batch sorption kinetics experiments were conducted. A nitrate solution (25 mg L^{-1}) was prepared by dissolving KNO_3 (ACS reagent; Bio Basic Inc., USA) in deionized water (18.2 MΩ cm^{-1} resistivity; Milli-Q Germany). The un-modified biochar and the MgO- and FeO-biochars were added to the NO_3 solution at the rate of 10 g L^{-1} in polypropylene centrifuge tubes. The tubes were then shaken on a horizontal shaker (Stuart orbital shaker, UK) at a constant speed of 250 rpm. The samples of each treatment were withdrawn at specific time intervals of 5, 15, 30, 60 and 120 min. After filtration, the NO_3 concentrations of the supernatant solutions were analyzed calorimetrically using the nitrophenol-disulfonic acid yellow color method (Jackson 1973). These kinetic batch experiments were conducted at initial pHs of 2, 4, 6 and 8. The following five different kinetic models were applied to describe the adsorption of NO_3 using each sorbent:

$$\text{First order}: \ln q_t = \ln q_e - k_1 t$$

$$\text{Pseudo-second order (Type 1)}: t/q_t = 1/k_2 q_e^2 + 1/q_e t$$

$$\text{Pseudo-second order (Type 2)}: 1/q_t = (1/k_2 q_e^2)1/t + 1/q_e t$$

$$\text{Pseudo-second order (Type 3)}: qt = q_e - (1/k_2 q_e)(q_t/t)$$

$$\text{Pseudo-second order (Type 4)}: q_t/t = k q_e^2 - k_2 q_e q_t$$

$$\text{Power function}: \ln qt = \ln b + k_f(\ln t)$$

where q_t and q_e are the amounts of NO_3 adsorbed by sorbents at time t and 0 min, respectively; k_1 is first-order rate constant; k_2 is the pseudo-second-order rate constant; k_f is rate coefficient value; and b is constant.

Sorption isotherms

To obtain sorption isotherms, batch sorption experiments were conducted at the NO_3 concentration range of 1–200 mg L^{-1}. The conocarpus biochars were equilibrated with NO_3 solution (pH 6) in polypropylene centrifuge tubes at an adsorbent dose of 10 g L^{-1} for 2 h at room temperature. After equilibration, the solutions were filtered, and the NO_3 concentrations in the supernatant were determined by colorimetry. Sorption isotherm parameters were obtained by using the linear, Langmuir and Freundlich isotherms as indicated by the following equations:

$$\text{Linear}: C_s = K_d C_e$$
$$\text{Langmuir}: C_e/C_s = 1/(K_b) + C_e/b$$
$$\text{Freundlich}: \log C_s = \log K_f + (1/n)\log C_e$$

where C_e: equilibrium solution-phase concentration (mmol L^{-1}), C_s: equilibrium solid-phase concentration (mmol kg^{-1}), K_d: linear distribution coefficient computed from the slope of the isotherm line (L kg^{-1}), b: Langmuir isotherm sorption capacity (mmol kg^{-1}), K_b: enthalpy-related sorption constant (L $mmol^{-1}$), n: sorption intensity constant and K_f: sorption capacity constant (L $mmol^{-1}$).

Results and discussion

Surface structure morphology of biochars

The surface structural characteristics of different biochars are presented in Table 1. The BET surface area of MgO-biochar was the highest (391.8 m^2 g^{-1}) followed by biochar (334.6 m^2 g^{-1}) and FeO-biochar (260.5 m^2 g^{-1}). Generally, biochars produced at high pyrolysis temperature (>450 °C) possess high surface area (Ahmad et al. 2014a). Relatively, the high surface area of MgO-biochar could be due to the reactive or light-burned MgO (magnesia) resulting from pyrolysis at 600 °C (Liu et al. 2007). Additionally, the smaller particle size (15.31 nm) of MgO-biochar also contributed to its high surface area (Khadka et al. 2014). The surface area of FeO-biochar was lower than biochar probably because of the abundance of FeO, which has a small surface area (Chen et al. 2011). The decrease in the pore volume of chemically modified biochars compared with un-modified biochar could be attributed to the blockage of pores by FeO and MgO (Downie et al. 2009). The SEM images clearly indicated the rough and porous surfaces of biochars (Fig. 1). Specifically, the FeO and MgO particles were uniformly deposited on the chemically modified biochar surfaces (Fig. 1b, c). The XRD patterns further confirmed the presence of Fe and Mg crystal phases in the chemically modified biochars (Fig. 2). Calcite ($CaCO_3$) was observed as the prevailing mineral in the un-modified biochar, which could be related to characteristics of the feedstock. The conocarpus plant is generally grown in calcareous soils, thus comprising large contents of $CaCO_3$, which was apparent in its derived biochar. The XRD pattern of FeO-biochar showed that Fe particles mainly corresponded to magnetite (Fe_3O_4) and FeO. Likewise, in the MgO-biochar, magnesia (MgO) was the foremost mineral phase.

FTIR spectroscopic assignments of un-modified and chemically modified biochars are shown in Fig. 3. Two broadbands at 3431 and 1106 cm^{-1} were assigned to hydroxyl (–OH) and organic siloxane (Si–O–C) functional groups, respectively. Several smaller combination bands from 2000 to 1660 and 1600 cm^{-1} presented aromatic ring groups and aromatic C=O and C=C functional groups, respectively (Coates 2000). A strong

Table 1 Surface structural characteristics of un-modified and chemically modified biochars

	Surface area (m^2 g^{-1})	Pore volume (cm^3 g^{-1})	Pore size (nm)	Particle size (nm)
Biochar	334.6	0.021	1.858	17.93
FeO-biochar	260.5	0.017	1.857	23.03
MgO-biochar	391.8	0.012	1.856	15.31

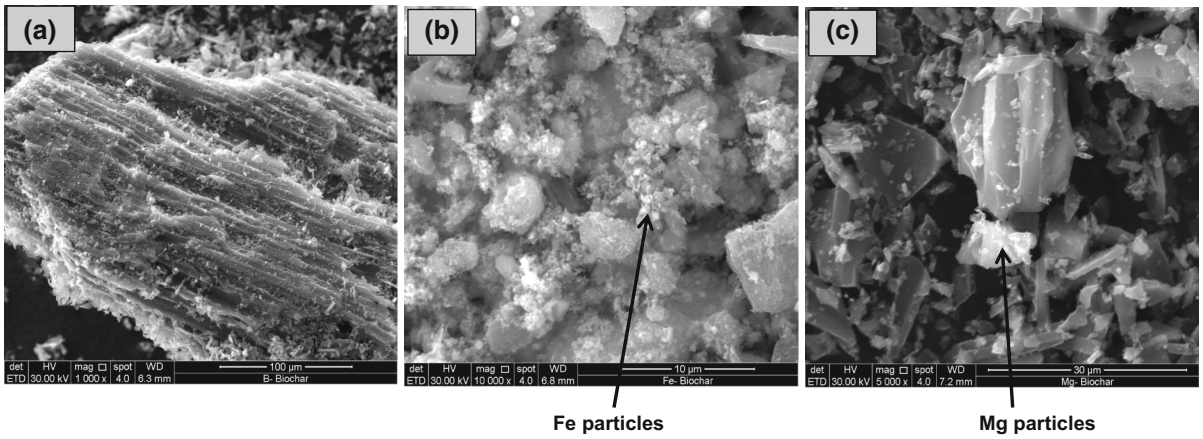

Fig. 1 Scanning electron microscopic photographs of **a** biochar, **b** FeO-biochar and **c** MgO-biochar

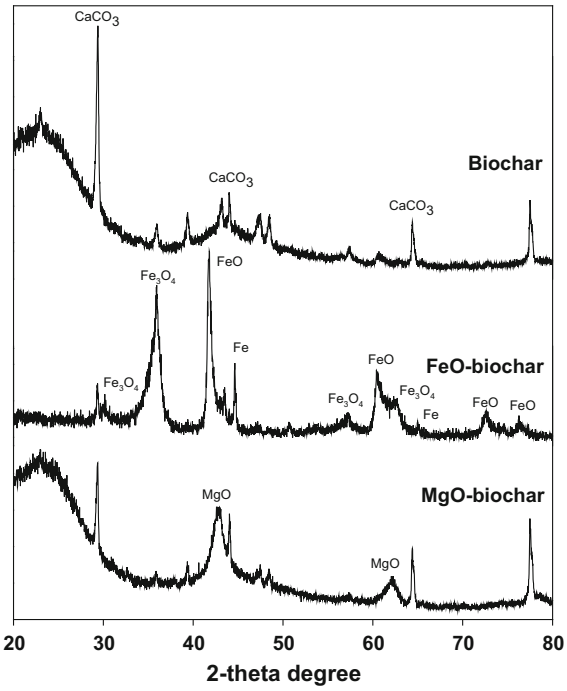

Fig. 2 XRD patterns of un-modified and chemically modified biochars

band at 1435 cm^{-1} was assigned to inorganic carbonate (CO_3) in the un-modified biochar that became less intense in the chemically modified FeO- and MgO-biochars. The presence of CO_3 was also confirmed in the XRD pattern (Fig. 2). A unique band at approximately 555 cm^{-1} in FeO-biochar was assigned to iron oxide (Chen et al. 2011).

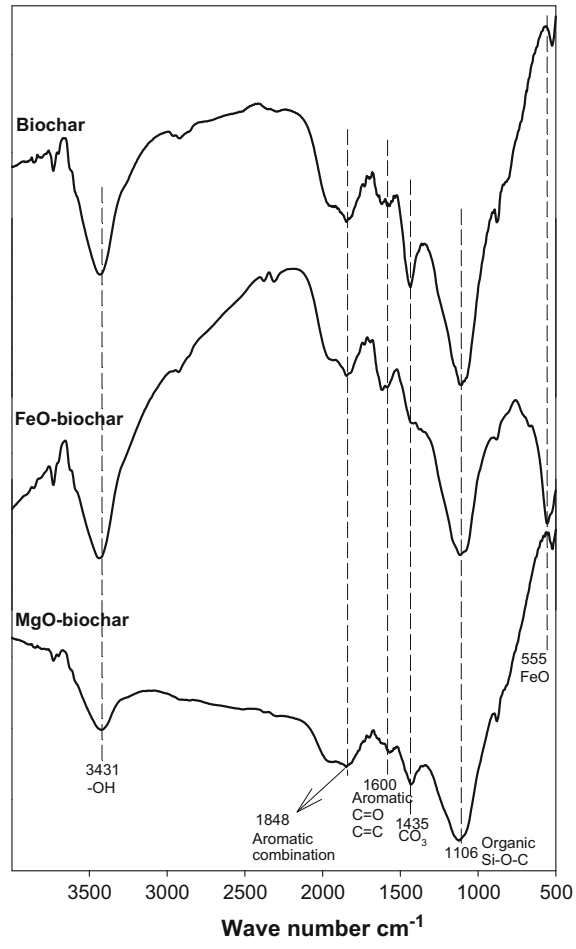

Fig. 3 FTIR spectroscopic assignments of un-modified and chemically modified biochars

Adsorption isotherms

The equilibrium sorption isotherm is a very important tool for designing sorption systems (Usman et al. 2013; Dogan et al. 2000). The synthesized un-modified and chemically modified biochars were tested for their sorption efficiency toward NO_3 removal from aqueous solutions. The sorption experiment was carried out at a NO_3 concentration range from 1 to 100 ppm (0.016–1.61 mmol L^{-1}) and an initial solution pH of 6. The adsorption data of this study were evaluated using the linear, Langmuir and Freundlich isotherms; the calculated isotherm parameters are given in Table 2. Overall, the linear model was not suitable for explaining the adsorption process of NO_3 onto all biochars, as indicated by small correlation coefficients ($R^2 = 0.620$–0.795). The results indicated that the adsorption data for NO_3 onto all three sorbents could generally be described by the Langmuir model with R^2 of 0.993–0.998 (Table 2), which indicates a monolayer and homogeneous/uniform adsorption. The Langmuir sorption parameters of all three biochars showed differences among the NO_3 adsorption, reflecting on their adsorption maxima (b) and bonding energy coefficient (k). The Langmuir maximum NO_3 sorption capacity of the MgO-biochar amounted to 45.36 mmol kg^{-1}, which is much higher than those of biochar (16.47 mmol kg^{-1}) and FeO-biochar (20.27 mmol kg^{-1}). The greater sorption capacity of MgO-biochar was due to its high surface area (Table 1) induced by thermal pyrolytic calcination of MgO particles. Moreover, it can be postulated that the attachment of MgO onto the surface of biochar could result in much stronger complexes between NO_3 and the MgO-biochar than those of biochar and FeO-biochar. Another plausible explanation for greater NO_3 sorption capacity of chemically modified biochars compared with un-modified biochar could be the electrostatic anionic attraction on the H_2^+–O–M-biochar, where M is either Mg or Fe (Ahmad et al. 2014a).

The sorption isotherms for NO_3 ions onto the investigated sorbents are shown in Fig. 4. The results showed high NO_3 ion adsorption at low initial NO_3 concentration and tended to increase with an increase in initial NO_3 concentration until equilibrium was achieved. The NO_3 adsorption onto biochars can be described by the L-type isotherm. The L-shaped adsorption isotherm could be explained by the high affinity of the adsorbent for the adsorptive at low concentrations, which then decreases as concentration increases. As the initial NO_3 concentration increased, the adsorption onto all biochars reached or tended to reach the maximum adsorption, suggesting that the available binding sites in the investigated sorbents resulted in the NO_3 adsorption; when these available binding sites were occupied, the adsorption capacity inclined to decrease at higher initial NO_3 concentration.

Adsorption kinetics

To evaluate the kinetics of the adsorption process, various kinetic models (first-order, different types of pseudo-second-order and power function) were applied to describe the mechanism of NO_3 removal using biochars. The values of equilibrium time were found to be 30–60 min among various treatments. The change in the rate of NO_3 ion removal might be because all adsorbent sites were initially vacant and the solute concentration gradient is high. The kinetic models parameters are presented in Table 3. It was found that Type 1 pseudo-second-order kinetics provided a better fit to the experimental data. The correlation coefficients for the linear plots of t/qt against time from the Type 1 pseudo-second-order rate law (Fig. 5) were >0.950 for all biochar systems at the contact time of 120 min. Therefore, the Type 1

Table 2 Linear, Langmuir and Freundlich isotherm parameters for NO_3 sorption onto different biochars

Sorbents	Linear			Langmuir			Freundlich			
	K_L	m	R^2	b (mmol kg^{-1})	k (L $mmol^{-1}$)	R^2	$1/n$	n	k_f	R^2
Biochar	8.20	5.42	0.620	16.47	8.03	0.998	0.550	1.82	18.32	0.903
MgO-biochar	26.5	7.81	0.795	45.36	3.49	0.993	0.553	1.81	20.90	0.875
FeO-biochar	10.7	5.10	0.783	20.27	5.64	0.997	0.567	1.76	20.33	0.926

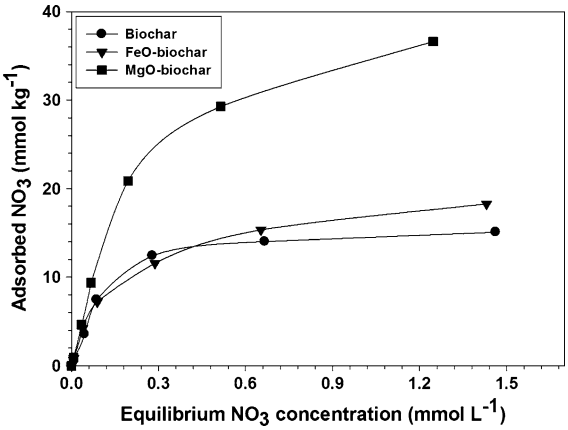

Fig. 4 Sorption isotherms of NO_3 onto un-modified and chemically modified biochars

pseudo-second-order expression reasonably predicted the maximum equilibrium sorption (q_e) and rate constant (k_2) values theoretically for all of the range of initial NO_3 concentrations studied. The q_e values for the Type 1 pseudo-second-order kinetic model ranged from 8.35 to 44.2 mmol kg^{-1} at different solution pHs. The MgO-biochar showed the highest equilibrium sorption capacity compared with other biochars at the initial solution pH of 4, 6 and 8, which is consistent with the Langmuir maximum adsorption capacity (Table 2). Similarly, the k_2 values were also high for the MgO-biochar at all of the pH values. k_2 is a time-scaling factor used to determine the time required to reach equilibrium (Ahmad et al. 2013b). The higher rate constant for MgO-biochar indicated that

Table 3 Kinetic model parameters for NO_3 sorption onto the sorbents

pH	Sorbents	First-order			Type 1 pseudo-second-order				Type 2 pseudo-second-order			
		q	K_1	R^2	q_e	K_2	h	R^2	q_e	K_2	h	R^2
2	Biochar	20.4	0.006	0.282	38.5	0.004	3E−06	0.999	56.50	8E−04	3E−07	0.932
	MgO-biochar	23.5	0.005	0.295	39.7	0.005	3E−06	0.996	49.50	0.002	6E−07	0.935
	FeO-biochar	17.5	0.009	0.289	44.2	0.002	9E−07	0.960	120.0	1E−04	7E−09	0.929
4	Biochar	6.57	0.006	0.749	13.7	0.006	3E−05	0.989	11.50	0.015	0.0001	0.887
	MgO-biochar	23.9	0.001	0.743	26.7	0.028	4E−05	1.000	25.97	0.062	9E−05	0.718
	FeO-biochar	7.63	0.005	0.738	13.8	0.009	5E−05	0.996	12.12	0.019	0.0001	0.890
6	Biochar	7.03	0.006	0.791	13.5	0.007	4E−05	0.992	11.10	0.023	0.0002	0.745
	MgO-biochar	18.6	0.001	0.618	21.1	0.036	8E−05	1.000	20.75	0.054	1E−04	0.861
	FeO-biochar	6.12	0.006	0.766	12.8	0.007	4E−05	0.987	10.40	0.019	0.0002	0.974
8	Biochar	7.02	0.004	0.505	10.3	0.025	0.0002	1.000	10.40	0.022	0.0002	0.998
	MgO-biochar	17.2	9E−04	0.441	18.9	0.075	2E−04	1.000	18.94	0.060	2E−04	0.973
	FeO-biochar	6.14	0.003	0.393	8.35	0.045	0.0007	1.000	8.760	0.028	0.0004	0.984

pH	Sorbents	Type 3 pseudo-second-order				Type 4 pseudo-second-order				Power function		
		q_e	K_2	h	R^2	q_e	K_2	h	R^2	k_f	b	R^2
2	Biochar	62.90	6E−04	2E−07	0.932	58.7	8E−04	2E−07	0.328	0.362	8.22	0.649
	MgO-biochar	52.60	0.001	5E−07	0.935	51.0	0.001	6E−07	0.536	0.292	11.3	0.658
	FeO-biochar	198.0	4E−05	9E−10	0.929	119	1E−04	8E−09	0.054	0.499	5.02	0.654
4	Biochar	12.10	0.012	9E−05	0.887	13.0	0.009	5E−05	0.751	0.271	3.59	0.952
	MgO-biochar	26.40	0.043	6E−05	0.718	0.63	1.76	4.42	0.795	0.043	21.7	0.921
	FeO-biochar	12.60	0.015	1E−04	0.890	13.1	0.012	7E−05	0.794	0.225	4.60	0.965
6	Biochar	12.10	0.014	1E−04	0.745	12.8	0.011	7E−05	0.633	0.229	4.26	0.927
	MgO-biochar	20.90	0.045	1E−04	0.861	21.0	0.044	1E−04	0.846	0.055	16.4	0.914
	FeO-biochar	11.30	0.013	1E−04	0.794	12.3	0.009	6E−05	0.653	0.265	3.40	0.930
8	Biochar	10.40	0.022	0.0002	0.823	10.5	0.022	2E−04	0.596	0.184	4.52	0.877
	MgO-biochar	19.00	0.058	2E−04	0.973	19.0	0.058	2E−04	0.965	0.048	15.3	0.826
	FeO-biochar	8.800	0.027	0.0004	0.984	8.74	0.028	4E−04	0.957	0.160	4.13	0.779

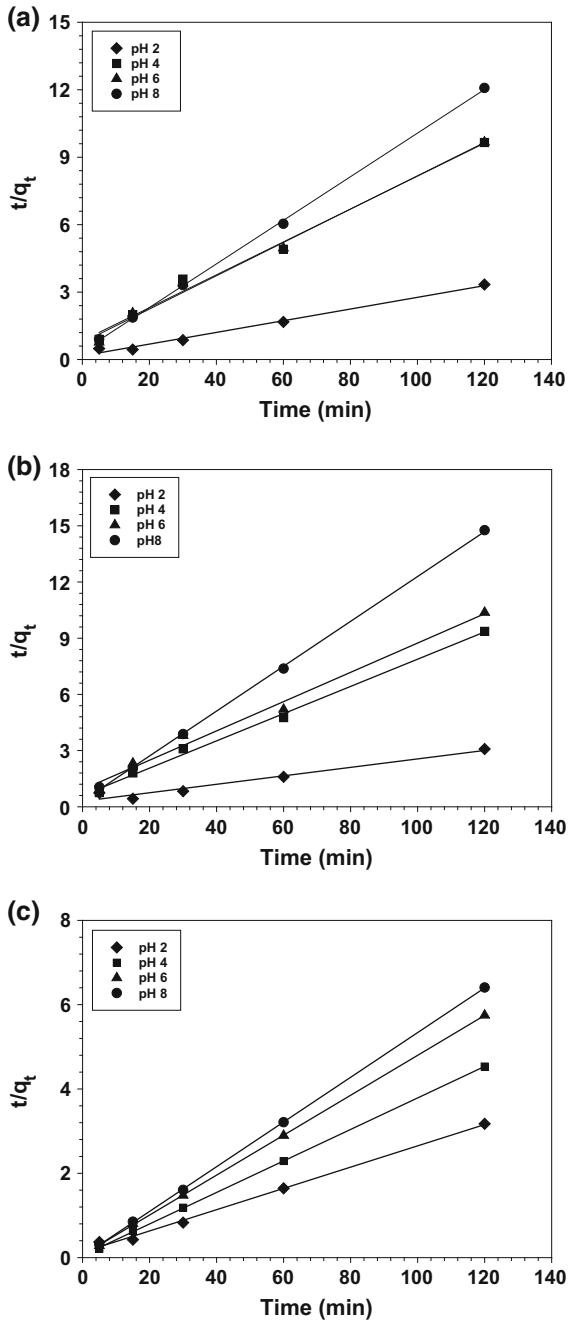

Fig. 5 Type 1 pseudo-second-order kinetic isotherms of NO_3 sorption onto **a** biochar, **b** FeO-biochar and **c** MgO-biochar at different pHs

maximum sorption was achieved in a shorter time than for other biochars (Plazinski et al. 2009).

Our results suggested that the pseudo-second-order model provided the best correlation of the NO_3 sorption kinetics data onto biochar systems, assuming that the rate-limiting step may be chemical sorption or chemisorption involving valency forces through sharing or exchange of electrons between biochars and NO_3. The smaller R^2 values for first-order, Types 2–4 pseudo-second-order and power function models implied that these models may not be appropriate for representing the experimental data of NO_3 sorption onto the investigated biochars. Therefore, by the linear method, a theoretical pseudo-second-order model was found to aptly represent the experimental data based on the Type 1 pseudo-second-order kinetic expression.

Removal efficiency and sorptive capacity

The removal efficiency of biochars for NO_3 ions at different equilibrium concentrations and pH values is shown in Fig. 6. The removal efficiency appears to depend on solution pH, initial NO_3 concentration and biochar type. Generally, regardless of initial NO_3 concentration and pH of the solution, the removal efficiency for NO_3 ions followed the order of MgO-biochar > FeO-biochar > biochar. The percentage removal was also affected by the initial NO_3 concentration and pH of the aqueous solution. The most effective pH value for nitrate removal was 2 for the investigated sorbents. Specifically, at an initial pH of 2 and at the initial NO_3 concentration of 50 mg L^{-1}, the percentage removal amounted to 89.1, 93.8 and 96.6 % for biochar, MgO-biochar and FeO-biochar, respectively. However, this removal efficiency tended to decrease with increasing values of initial pH, reaching 20.2, 24.6 and 46.5 % at the highest initial pH of 8 for FeO-biochar, biochar and MgO-biochar, respectively. The highest NO_3 removal at the lower pH is mainly due to the reduction in negative charges on the surface of sorbents by the excess of protons in solutions (Öztürk and Bektas 2004); subsequently, the number of positively charged sites increases. Generally, a positively charged surface site on the adsorbent favors the adsorption of anions due to electrostatic attraction (Öztürk and Bekta 2004).

The results showed that the percentage removal of NO_3 was also affected by initial NO_3 concentration. Generally, the percentage removal of NO_3 decreased with increasing initial ionic concentration. The percentage removal of NO_3 was 52.7–56.0 % at the initial ionic concentration of 1 mg L^{-1} for all of the sorbents, and this removal efficiency reduces to

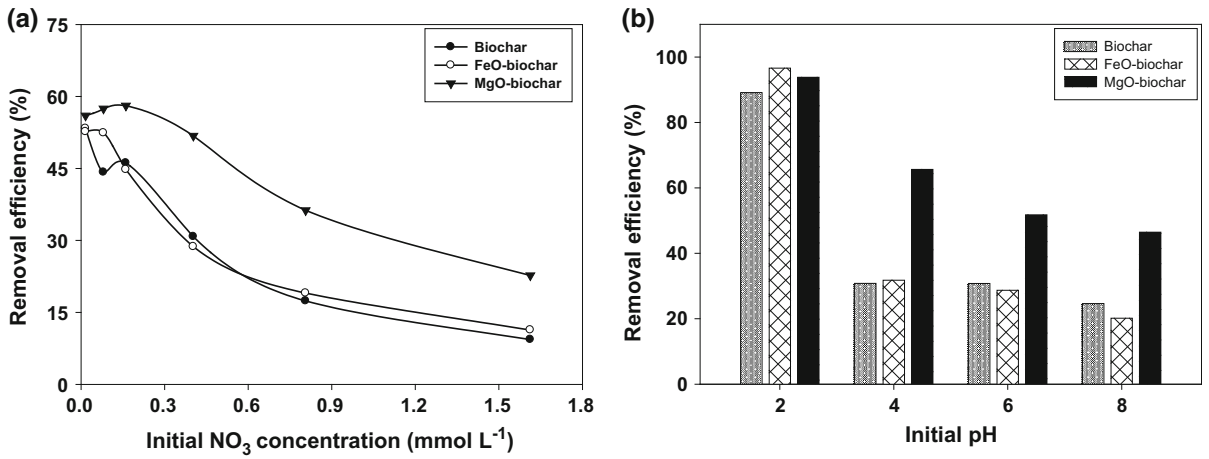

Fig. 6 Removal efficiency of different biochars with increasing **a** initial NO_3 concentration and **b** initial solution

44.2–57.5, 44.8–58, 28.7–51.8, 14.4–36.3 and 9.3–22.7 % at initial concentrations of 5, 10, 25, 50 and 100 mg L^{-1}, respectively. A higher adsorption at lower initial concentration may be due to the high adsorption affinity between the NO_3 ions and the biochar. At higher initial concentrations, the availability of binding sites for adsorbing NO_3 ions might tend to decrease, preventing further adsorption of NO_3 ions on the adsorbent surfaces.

The removal efficiency of MgO-biochar was much higher than that of other biochars in most cases, indicating that the surface modifications induced by MgO onto the biochar resulted in enhanced NO_3 adsorption. It has been reported that metal oxides have a large binding capacity for negatively charged ions, such as phosphate and arsenate (Manning and Goldberg 1996). The surface of metal oxide in the presence of water becomes hydroxylated, resulting in either a positive or negative surface charge, which is dependent upon the solution pH. The point of zero charge of MgO is very high (12), suggesting a positively charged surface in most natural aqueous conditions (Yao et al. 2011). In a study conducted by Zhang et al. (2012), the removal of anions from aqueous solutions by MgO-biochar nanocomposites could be attributed to mono-, bi- and tri-nuclear complexions. Consequently, MgO particles in the biochar matrix could result in high aqueous anions removal efficiency, showing a suggestive trend toward wastewater remediation.

Conclusions

Conocarpus green waste was subjected to chemical modification with Mg and Fe oxides to produce biochars via thermal pyrolysis. A dramatic increase in the specific surface area of MgO-biochar was achieved. The un-modified and chemically modified biochars were assessed for the removal of NO_3 ions from aqueous solutions. The best fitting of the sorption experimental data to the Langmuir and Type 1 pseudo-second-order kinetic models predicted that MgO-biochar was the most effective in NO_3 sorption due to its high surface area and strong ionic complexation through chemisorption. The results demonstrated that chemical modification of biochar could advance the efforts for achieving more efficient biochar. However, future investigations are required to test chemically modified biochars in real-time contaminated water.

Acknowledgments The authors extend their appreciation to the Deanship of Scientific Research, King Saud University, for funding this work through the international research group Project IRG-14-14.

References

Ahmad, M., Lee, S. S., Dou, X., Mohan, D., Sung, J. K., Yang, J. E., & Ok, Y. S. (2012). Effects of pyrolysis temperature on soybean stover- and peanut shell-derived biochar properties and TCE adsorption in water. *Bioresource Technology, 118*, 536–544.

Ahmad, M., Lee, S. S., Oh, S. E., Mohan, D., Moon, D. H., Lee, Y. H., & Ok, Y. S. (2013a). Modeling adsorption kinetics of trichloroethylene onto biochars derived from soybean stover and peanut shell wastes. *Environmental Science and Pollution Research, 20*, 8364–8373.

Ahmad, M., Lee, S. S., Rajapaksha, A. U., Vithanage, M., Zhang, M., Cho, J. S., et al. (2013b). Trichloroethylene adsorption by pine needle biochar produced at various pyrolysis temperatures. *Bioresource Technology, 143*, 615–622.

Ahmad, M., Rajapaksha, A. U., Lim, J. E., Zhang, M., Bolan, N., Mohan, D., et al. (2014a). Biochar as a sorbent for contaminant management in soil and water: A review. *Chemosphere, 99*, 19–33.

Ahmad, M., Vithanage, M., Kim, K., Cho, J. S., Lee, Y. H., Joo, Y. K., et al. (2014b). Inhibitory effect of veterinary antibiotics on denitrification in groundwater: A microcosm approach. *The Scientific World Journal.* ID: 879831. doi:10.1155/2014/879831.

Al-Wabel, M. I., Al-Omran, A., El-Naggar, A. H., Nadeem, M., & Usman, A. R. A. (2013). Pyrolysis temperature induced changes in characteristics and chemical composition of biochar produced from conocarpus waste. *Bioresource Technology, 131*, 374–379.

Aly, A. A., Hasan, Y. N. Y., & Al-Farraj, A. S. (2014). Olive mill wastewater treatment using a simple zeolite-based low-cost method. *Journal of Environmental Management, 145*, 341–348.

Bagherifam, F., Komarneni, S., Lakzian, A., Fotovat, A., Khorasani, R., Huang, W., et al. (2014). Highly selective removal of nitrate and perchlorate by organoclay. *Applied Clay Science, 95*, 126–132.

Camargo, J. A., Alonso, A., & Salamanca, A. (2005). Nitrate toxicity to aquatic animals: A review with new data for freshwater invertebrates. *Chemosphere, 58*, 1255–1267.

Chen, B., Chen, Z., & Lv, S. (2011). A novel magnetic biochar efficiently sorbs organic pollutants and phosphate. *Bioresource Technology, 102*, 716–723.

Coates, J. (2000). Interpretation of infrared spectra, a practical approach. In R. A. Meyers (Ed.), *Encyclopedia of analytical chemistry* (pp. 10815–10837). Chichester: Wiley.

Dogan, M., Alkan, M., & Onganer, Y. (2000). Adsorption of methylene blue from aqueous solution onto perlite. *Water, Air, and Soil Pollution, 120*, 229–248.

Downie, A., Crosky, A., & Munroe, P. (2009). Physical properties of biochar. In J. Lehmann & S. Joseph (Eds.), *Biochar for environmental management science and technology* (pp. 13–32). London: Earthscans.

Jackson, M. L. (1973). *Soil chemical analysis*. New Delhi: Prentice Hall of India Pvt. Ltd.

Jing, X. R., Wang, Y. Y., Liu, W. J., Wang, Y. K., & Jiang, H. (2014). Enhanced adsorption performance of tetracycline in aqueous solutions by methanol-modified biochar. *Chemical Engineering Journal, 248*, 168–174.

Kassaee, M. Z., Motamedi, E., Mikhak, A., & Rahnemaie, R. (2011). Nitrate removal from water using iron nanoparticles produced by arc discharge vs. reduction. *Chemical Engineering Journal, 166*, 490–495.

Keshavarzi, B., Moore, F., Najmeddin, A., Rahmani, F., & Malekzadeh, A. (2012). Quality of drinking water and high incidence rate of esophageal cancer in Golestan province of Iran: A probable link. *Environmental Geochemistry and Health, 34*, 15–26.

Khadka, P., Ro, J., Kim, H., Kim, I., Kim, J. T., Kim, H., et al. (2014). Pharmaceutical particle technologies: An approach to improve drug solubility, dissolution and bioavailability. *Asian Journal of Pharmaceutical Sciences,*. doi:10.1016/j.ajps.2014.05.005.

Lehmann, J., & Joseph, S. (2009). Biochar for environmental management: An introduction. In J. Lehmann & S. Joseph (Eds.), *Biochar for environmental management science and technology* (pp. 1–12). London: Earthscans.

Liu, B., Ray, A. S., & Thomas, P. S. (2007). Strength development in autoclaved aluminosilicate rich industrial waste-cement systems containing reactive magnesia. *Journal of Australian Ceramics Society, 43*, 82–87.

Liu, C. W., Lin, C. N., Jang, C. S., Ling, M. P., & Tsai, J. W. (2011). Assessing nitrate contamination and its potential health risk of Kinmen residents. *Environmental Geochemistry and Health, 33*, 503–514.

Loni, O. A., Zaidi, F. K., Alhumimidi, M. S., Alharbi, O. A., Hussein, M. T., Dafalla, M., et al. (2014). Evaluation of groundwater quality in an evaporation dominant arid environment: A case study from Al Asyah area in Saudi Arabia. *Arabian Journal of Geosciences,*. doi:10.1007/s12517-014-1623-4.

Ma, Y., Liu, W. J., Zhang, N., Li, Y. S., Jiang, H., & Sheng, G. P. (2014). Polyethylene amine modified biochar adsorbent for hexavalent chromium removal from the aqueous solution. *Bioresource Technology, 169*, 403–408.

Manning, B. A., & Goldberg, S. (1996). Modeling competitive adsorption of arsenate with phosphate and molybdate on oxide minerals. *Soil Science Society of America Journal, 60*, 121–131.

Mayer, Z. A., Eltom, Y., Stennett, D., Schroder, E., Apfelbacher, A., & Hornung, A. (2014). Characterization of engineered biochar for soil management. *Environmental Progress and Sustainable Energy, 33*, 490–496.

Mohan, D., Kumar, H., Sarswat, A., Franco, M. A., & Pitmann, C. U, Jr. (2014). Cadmium and lead remediation using magnetic oak wood and oak bark fast pyrolysis bio-chars. *Chemical Engineering Journal, 236*, 513–528.

Öztürk, N., & Bektas, T. E. (2004). Nitrate removal from aqueous solution by adsorption onto various materials. *Journal of Hazardous Materials, 112*, 155–162.

Plazinski, W., Rudzinski, W., & Plazinska, A. (2009). Theoretical models of sorption kinetics including a surface reaction mechanism: A review. *Advances in Colloid and Interface Science, 152*, 2–13.

Rajapaksha, A. U., Vithanage, M., Zhang, M., Ahmad, M., Mohan, D., Chang, S. X., & Ok, Y. S. (2014). Pyrolysis condition affected sulfamethazine sorption by tea waste biochars. *Bioresource Technology, 166*, 303–308.

Rodríguez-Marotoet, J. M., García-Herruzo, F., García-Rubio, A., Gomez-Lahoz, C., & Vareda-Alonso, C. (2009). Kinetics of the chemical reduction of nitrate by zero-valent iron. *Chemosphere, 74*, 804–809.

Shackley, S., Hammond, J., Gaunt, J., & Ibarrola, R. (2011). The feasibility and costs of biochar deployment in the UK. *Carbon Management, 2*, 335–356.

Sowmya, A., & Meenakshi, S. (2014). Effective removal of nitrate and phosphate anions from aqueous solutions using

functionalised chitosan beads. *Desalination and Water Treatment, 52*, 2583–2593.

Usman, A. R. A., Sallam, A. S., Al-Omran, A., El-Naggar, A. H., Alenazi, K. K. H., Nadeem, M., & Al-Wabel, M. I. (2013). Chemically modified biochar produced from conocarpus wastes: An efficient sorbent for Fe(II) removal from acidic aqueous solutions. *Adsorption Science and Technology, 31*, 625–640.

Vithanage, M., Rajapaksha, A. U., Zhang, M., Thiele-Bruhn, S., Lee, S. S., & Ok, Y. S. (2014). Acid-activated biochar increased sulfamethazine retention in soils. *Environmental Science and Pollution Research,*. doi:10.1007/s11356-014-3434-2.

Wang, T., Lin, J., Xhen, Z., Megharaj, M., & Naidu, R. (2014). Green synthesized iron nanoparticles by green tea and eucalyptus leaves extracts used for removal of nitrate in aqueous solution. *Journal of Cleaner Production, 83*, 413–419.

WHO. (2011). *Guidelines for drinking water quality* (4th ed.). Geneva: World Health Organization.

Yao, Y., Gao, B., Inyang, M., Zimmerman, A. R., & Cao, X. (2011). Removal of phosphate from aqueous solution by biochar derived from anaerobically digested sugar beet tailings. *Journal of Hazardous Materials, 190*, 501–507.

Zhang, M., Gao, B., Yao, Y., Xue, Y., & Inyang, M. (2012). Synthesis of porous MgO-biochar nanocomposites for removal of phosphate and nitrate from aqueous solutions. *Chemical Engineering Journal, 210*, 26–32.